Circulation Reports
Circ Rep 2019; 1: 199–205
doi:10.1253/circrep.CR-18-0012

ORIGINAL ARTICLE
Aortic Disease

Aortic Strain Correlates With Elastin Fragmentation in Fibrillin-1 Hypomorphic Mice

Jeff Z. Chen, BSc; Hisashi Sawada, MD, PhD; Jessica J. Moorleghen, BSc; Mackenzie Weiland, BSc; Alan Daugherty, PhD; Mary B. Sheppard, MD

Background: High-frequency ultrasound has facilitated in vivo measurement of murine ascending aorta, allowing aortic strain to be determined from 2-D imaging. Thoracic aortic aneurysms associated with mutations in *fibrillin-1* (*FBN1*) display elastin fragmentation, which may affect aortic strain. In this study, we determined the relationship between elastin fragmentation and aortic circumferential strain in wild-type (WT) and fibrillin-1 hypomorphic (*FBN1*$^{mgR/mgR}$) mice.

Methods and Results: Luminal diameter of the ascending aorta from WT and *FBN1*$^{mgR/mgR}$ mice was measured in systole and diastole. Expansion of the ascending aorta during systole in male and female WT mice was 0.21±0.02 mm (16.3%) and 0.21±0.01 mm (17.0%), respectively, while expansion in male and female *FBN1*$^{mgR/mgR}$ mice was 0.11±0.04 mm (4.9%) and 0.07±0.02 mm (4.5%), respectively. Reduced circumferential strain was observed in *FBN1*$^{mgR/mgR}$ mice compared with WT littermates. Elastin fragmentation was inversely correlated to circumferential strain (R^2=0.628, P=0.004) and significantly correlated with aortic diameter (systole, R^2=0.397, P=0.038; diastole, R^2=0.515, P=0.013).

Conclusions: *FBN1*$^{mgR/mgR}$ mice had increased aortic diameter, reduced circumferential strain, and increased elastin fragmentation. Elastin fragmentation in *FBN1*$^{mgR/mgR}$ and their WT littermates was correlated with reduced circumferential strain.

Key Words: Circumferential strain; Elastin fragmentation; Marfan syndrome; Thoracic aortic aneurysm; Ultrasound

Thoracic aortic aneurysms (TAA) are abnormal dilations of the aorta associated with increased risk of life-threatening aortic dissection and rupture.[1] Although the majority of TAA have not yet been associated with a specific mutation, TAA often occur in the context of inherited genetic disorders such as Marfan syndrome. TAA tissues from patients with Marfan syndrome display decreased aortic elasticity.[2] Measurement of aortic diameter is a critical prognostic indicator because larger diameter is associated with higher risk of rupture.[1]

Mouse models of spontaneous TAA can be generated by systemic use of chemicals such as angiotensin II (AngII) or β-aminopropionitrile.[3,4] Mouse models of heritable TAA can be generated by manipulation of genes responsible for extracellular matrix integrity or smooth muscle cell function such as *fibrillin-1* (*FBN1*), *fibulin-4*, and *ACTA-2*.[5–9] In this study we used the *fibrillin-1* hypomorphic (*FBN1*$^{mgR/mgR}$) mouse model, in which TAA develops aggressively early in life. Previous studies in these mice have indicated decreased elastin expression and increased elastin fragmentation in aneurysmal tissue.[5,10–13] This elastin fragmentation may influence aortic circumferential strain. We hypothesized that vascular strain in the ascending aorta, measured on 2-D high-frequency ultrasound, correlated with elastin fragmentation. To test this hypothesis, we compared circumferential aortic strains in the *FBN1*$^{mgR/mgR}$ mice, which naturally develop elastin fragmentation, vs. sex-matched wild-type (WT) littermates.

Aortic diameter measurement is the primary endpoint for quantification of TAA severity in disease models. Previously, ascending aorta measurements in mice were limited to terminal endpoints.[14,15] This included measurement of aortic elasticity and sheer strain in ex vivo tissues.[10] Development of high-frequency ultrasound, in the range 40–50 MHz, has enabled resolution that distinguishes small changes of aortic dimension over sequential measurements.[16] This resolution allows measurements of circumferential strain from 2-D images captured in vivo and enables investigation of the impact of elastin fragmentation on aortic strain.

This study used 2-D, trans-thoracic ascending aortic ultrasound measurements of the ascending aorta in WT mice and their *FBN1*$^{mgR/mgR}$ littermates to measure circumferential strain in vivo. When standardized, the 2-D, trans-thoracic ascending aortic ultrasound measurement correlates closely with traditional ex vivo measurement and has low

Received November 20, 2018; revised manuscript received March 22, 2019; accepted April 1, 2019; J-STAGE Advance Publication released online April 27, 2019 Time for primary review: 23 days
Saha Cardiovascular Research Center (J.Z.C., H.S., J.J.M., M.W., A.D., M.B.S.), Department of Physiology (J.Z.C., A.D., M.B.S.), Department of Family and Community Medicine (M.B.S.), Department of Surgery (M.B.S.), University of Kentucky, Lexington, KY, USA
Mailing address: Mary B. Sheppard, MD, Saha Cardiovascular Research Center, BBSRB, Room 247, University of Kentucky, Lexington, KY 40536-0509, USA. E-mail: mary.sheppard@uky.edu
ISSN-2434-0790

Table. Characteristics of WT and *FBN1*$^{mgR/mgR}$ Mice

Sex / Genotype	n	Age at ultrasound (days)	Body weight (g)	SBP (mmHg)	Pulse rate (beats/min)	AoDs (mm)†	AoDd (mm)†	AoDs–AoDd (mm)‡
Male								
WT	8	74.8±1.0	25.7±0.5	147±7	506±23	1.50±0.05	1.29±0.05***	0.21±0.02
FBN1$^{mgR/mgR}$	8	74.8±1.0	26.2±0.8	139±18	524±31	2.35±0.13	2.24±0.15**	0.11±0.04*
Female								
WT	5	74.7±1.3	20.5±0.7	137±9	547±58	1.42±0.03	1.23±0.04***	0.21±0.01
FBN1$^{mgR/mgR}$	7	75.2±1.2	20.8±0.8	125±13	443±23	1.64±0.07	1.57±0.08**	0.07±0.02*

Data given as mean±SEM. P>0.05 between WT vs. *FBN1*$^{mgR/mgR}$ by Student's t-test. *P<0.05 WT vs. *FBN1*$^{mgR/mgR}$. **P<0.01, ***P<0.001, AoDs vs. AoDd. Male and female *FBN1* WT and *FBN1*$^{mgR/mgR}$ mice were aged to 11 weeks. Body weight was measured before ultrasonography. SBP and pulse rate were measured for 3 consecutive days using a tail cuff-based technique. No measurements were significantly different between WT and *FBN1*$^{mgR/mgR}$ within sex. †Male mice: WT P<0.001, *FBN1*$^{mgR/mgR}$ P=0.004; female mice: WT P<0.001, *FBN1*$^{mgR/mgR}$ P=0.009. ‡WT vs. *FBN1*$^{mgR/mgR}$: male mice, P=0.03; female mice, P=0.01. AoDd, aortic diameter in diastole; AoDs, aortic diameter in systole; *FBN1*, fibrillin-1; SBP, systolic blood pressure; WT, wild type.

interobserver variability.[17] Finally, we assessed the correlation of these findings with elastin fragmentation.

Methods

Mice

Male and female WT C57BL/6J and *FBN1*$^{mgR/mgR}$ littermates were generated at the Jackson Laboratory (Bar Harbor, ME, USA) from stock 005704. Heterozygous *FBN1*$^{mgR/+}$ male mice were bred with *FBN1*$^{mgR/+}$ female mice to generate mice of desired genotypes. Mice were fed standard laboratory diet and water ad libitum and maintained on a 14:10-h light:dark cycle. Mice were transferred to a barrier facility at the University of Kentucky. All protocols were approved by the University of Kentucky IACUC.

Non-Invasive Blood Pressure Measurement

Systolic blood pressure (SBP) was measured by tail cuff using a Kent Scientific Coda 8 as described previously.[18] All measurements were performed at the beginning of the light cycle. Briefly, mice were restrained and placed on a warming platform. Twenty cycles of blood pressure measurements were obtained for each mouse. Measurements <50 mmHg and >220 mmHg were excluded. Pulse rate <400 beats/min was excluded from calculation. SBP was measured on 3 consecutive days at the same time of day. Measurements represent the mean of 3 days.

Ultrasound Measurement

Ultrasound was carried out in WT and *FBN1*$^{mgR/mgR}$ mice at 11 weeks of age. Mice were anesthetized using isoflurane; dose was titrated at 2–3% wt/vol isoflurane with 2 L/min O_2 to maintain heart rate 400–500 beats/min as monitored on concurrent 3-lead electrocardiogram. Ultrasound cine-loops were captured using a Vevo 2100 system with a MicroScan MS550 40-MHz transducer (VisualSonics, Toronto, ON, Canada). Frame rate was ≥300 frames/s, and 300 frames were stored per cine-loop. Aortic images were acquired from a modified right parasternal long axis view (1–2 ribs caudal to the right parasternal long axis view; **Supplementary Figure 1**). The probe was angled 45° relative to the chest to avoid sternum artefacts. Images were standardized to include visualization of 2 anatomical landmarks: the innominate artery and aortic valve (**Supplementary Figure 2A**). The ascending aorta was defined as the region between the sinotubular junction and the innominate artery. The largest ascending aortic diameter was measured in both systole and diastole of 3 separate cardiac cycles for each mouse. To facilitate measurements, a center line was drawn on the acquired image at the midpoint between the aortic walls. Aortic diameter (AoD) was measured at the largest diameter perpendicular to the center line of the aorta (**Supplementary Figure 2B**). AoD in systole (AoDs) was measured at physiologic systole: when the aorta was maximally dilated. AoD in diastole (AoDd) was measured at the end of diastole: defined as during the R wave (**Supplementary Figure 2C**). Aortic images were analyzed by 2 independent observers blinded to the experimental groups. Circumferential strain was calculated as previously described using Equation 1.[19]

$$0.5\left[\left(\frac{AoDs}{AoDd}\right)^2-1\right]*100\% \qquad (1)$$

Ex Vivo Aorta Measurements

Mice were killed by overdose of ketamine:xylazine at 11 weeks of age followed by exsanguination via cardiac puncture and saline perfusion. The aorta was dissected away from surrounding tissue, and Optimal Cutting Temperature (OCT) Compound (Sakura Finetek, Torrance, CA, USA) was slowly introduced via the left ventricle to maintain aortic patency. A black plastic sheet was inserted behind the aorta and heart to increase contrast and facilitate visualization of aortic borders. The aorta was immediately imaged using a Nikon SMZ800 stereoscope and measurements were recorded using NIS-Elements AR 4.51 (Nikon Instruments, Melville, NY, USA). Fluid OCT maintained aortic patency to facilitate ex vivo and histologic analyses. Ascending aortic diameters were measured at the largest width perpendicular to the vessel.

Quantification of Elastin Fragmentation

Three proximal thoracic aortas per group were selected randomly and ≥9 tissue sections per aorta were generated using a cryostat. Tissue sections (10 μm) were generated from the aortic root to the aortic arch at 100-μm intervals. Three sections corresponding to the region of largest dilation between the sinotubular junction and the arch were analyzed. Briefly, elastin was visualized on auto-fluorescence at an excitation spectrum of 460–500 nm. Multiple high-magnification images were acquired of each section that were subsequently aggregated to a single image of the entire section using ImageJ.[20] Fragmentation was defined

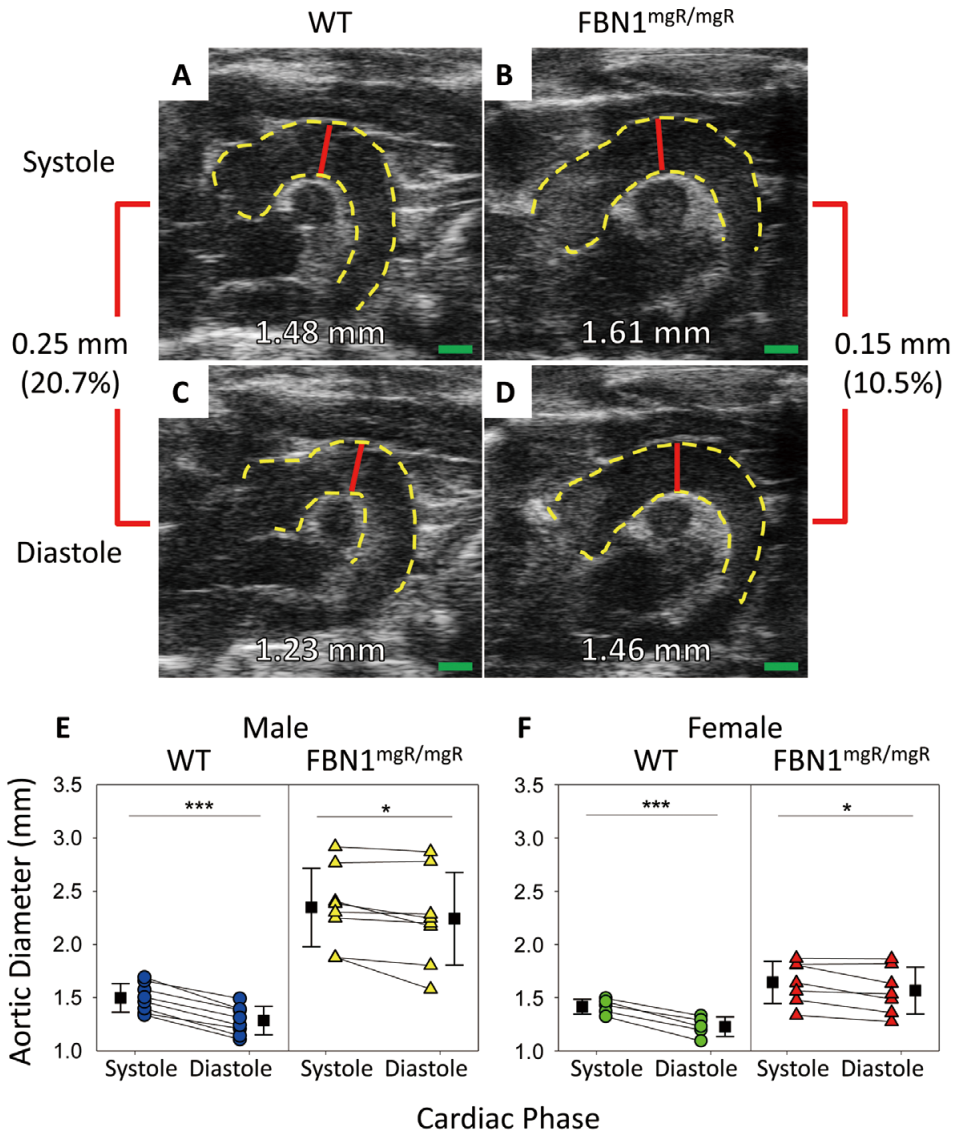

Figure 1. Effect of cardiac cycle on ascending aortic diameters. (**A**–**D**) Representative B-mode imaging of ascending aortas from 11-week-old wild-type (WT) and *fibrillin-1* (*FBN1*)$^{mgR/mgR}$ mice. (**E**,**F**) Quantification of aortic diameters in systole and diastole of (**E**) male and (**F**) female littermates. There were significant differences in aortic diameters between systole and diastole within both sex and genotype. Red line, region measured; green bar, 1 mm. Male, n=8 WT and 8 *FBN1*$^{mgR/mgR}$; female, n=5 WT and 7 *FBN1*$^{mgR/mgR}$; ***P<0.001, *P<0.05 between groups (paired Student's t-test).

as the presence of discernable breaks of continuous elastin fiber. The number of elastin breaks was counted by 2 independent investigators blinded to the sample identification. Individual data are represented as the mean number of elastin breaks per aortic section calculated by 2 independent investigators.

Statistical Analysis

Data are reported as mean±SEM. Statistical analysis was performed using SigmaPlot (Systat Software; San Jose, CA, USA). For 2-group comparisons, all data passed normality and equal variance tests. Paired Student's t-test was used to compare systole and diastole from the same mouse, and unpaired Student's t-test was used between groups. P<0.05 was considered statistically significant. Regression was calculated using Pearson's coefficient of correlation. Bland-Altman analysis was performed by plotting the mean of aortic diameter measured ex vivo and on ultrasound vs. the difference of aortic diameter measured ex vivo and on ultrasound, with negative values indicating that ex vivo measurements are smaller than ultrasound measurements (Equation 2). Bias and limits of agreement calculated for Bland-Altman analysis were used to compare measurements of the same biological variable obtained using 2 different measurement methods.

$$\textit{Difference Aortic Diameter} = \textit{ex vivo diameter} - \textit{ultrasound diameter} \quad (2)$$

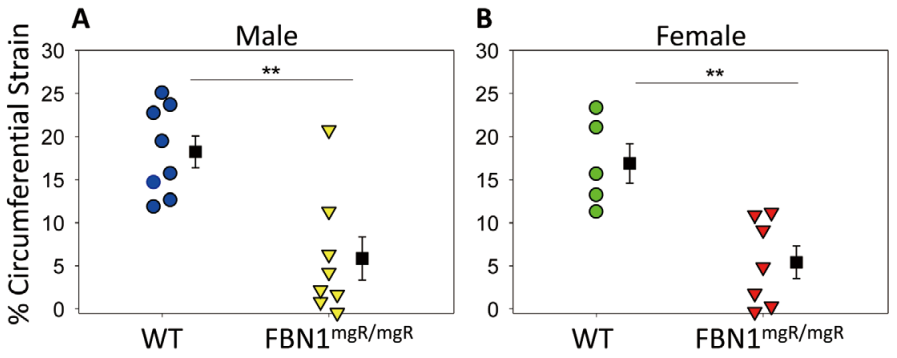

Figure 2. Circumferential Green-Lagrange strain of the aorta during cardiac cycle in wild-type (WT) and *fibrillin-1* (*FBN1*)$^{mgR/mgR}$ mice. Percent expansion was calculated by comparing aortic measurements between systole and diastole in a cardiac cycle. (**A**) Male and (**B**) female WT mice had greater percent expansion during the cardiac cycle compared with their *FBN1*$^{mgR/mgR}$ littermates. Male, n=8 WT and 8 *FBN1*$^{mgR/mgR}$; female, n=5 WT and 7 *FBN1*$^{mgR/mgR}$; **P<0.01 between groups (Student's t-test).

Results

Body Weight and SBP

The SBP and diastolic blood pressure were measured by tail cuff at 11 weeks of mice for 3 consecutive days before death at similar times of the day. Blood pressure was not significantly different in WT and *FBN1*$^{mgR/mgR}$ sex-matched littermates. In addition, body weight was not different between WT and *FBN1*$^{mgR/mgR}$ sex-matched littermates (**Table**). During ultrasonography, anesthesia was titrated to maintain a heart rate 400–500 beats/min. Therefore, heart rate was not significantly different between groups during ultrasonography (heart rate: WT, 453±27 beats/min; *FBN1*$^{mgR/mgR}$, 439±26 beats/min; P=0.86). Heart rate was also not different between groups during non-invasive blood pressure measurements (**Table**).

2-D Ultrasound Ascending Aorta Measurements

Ultrasound measurements of ascending aortas of 11-week-old male and female WT mice and their *FBN1*$^{mgR/mgR}$ littermates in systole and diastole were measured via the standardized protocol described herein (**Figure 1A–D**). Ascending aortic diameter measured in systole was significantly greater than that measured in diastole (**Figure 1E,F**) in both male and female mice (**Table**). The difference between systole and diastole in WT mice was larger than in *FBN1*$^{mgR/mgR}$ sex-matched littermates.

Circumferential Strain in Ascending Aorta During Systole

Fibrillin-1 hypomorphic mice had significantly less circumferential expansion during systole compared with their WT littermates. Green-Lagrange strain was calculated using aortic diameter on B-mode imaging during systole and diastole for each individual mouse, according to equation 1. Increased circumferential strain was observed in WT ascending aortas compared with aortas from *FBN1*$^{mgR/mgR}$ mice (**Figure 2**). This effect was seen in both male and female mice. For male mice: mean percent strain WT, 18.2±1.8%; *FBN1*$^{mgR/mgR}$, 5.9±2.4% (P=0.001). For female mice: mean percent strain WT, 17.4±1.9%; *FBN1*$^{mgR/mgR}$, 5.4±1.8% (P=0.001).

Elastin Fragmentation: Circumferential Strain and Aortic Diameter Correlations

As expected, aortic sections from *FBN1*$^{mgR/mgR}$ mice had significantly greater elastin fragmentation compared with their WT counterparts (**Figure 3A–C**). Elastin fragmentation was also significantly inversely correlated with in vivo circumferential strain (R^2=0.628, P=0.004) and positively correlated with both systolic and diastolic aortic diameters (systole, R^2=0.397, P=0.038; diastole, R^2=0.515, P=0.013; **Figure 3D–F**). On multiple linear regression modeling, we also determined that the *FBN1* genotype contributed significantly to differences in elastin fragmentation (P=0.001) and that elastin fragmentation did not correlate with sex (P=0.414).

Discussion

Previously, our group reported aortic diameters in aneurysm studies without specifying the cardiac phase during which these in vivo measurements were taken.[16,21–23] In this study, we have demonstrated that in vivo 2-D ultrasound measurements are accurate and correlate with in situ measurements of exposed aortas (**Supplementary Figure 3**). Furthermore, we quantified the difference between measurements taken in systole and diastole in the thoracic aorta (**Figure 1**). This suggested that 2-D trans-thoracic ultrasound can be used to calculate circumferential aortic strain, despite the fact that the thoracic aorta experiences increased longitudinal displacement due to its proximity to the beating heart.[19,24] Using a mouse model of elastin fragmentation, we further investigated whether differences in aortic strain between *FBN1*$^{mgR/mgR}$ mice and their WT littermates correlated with elastin fragmentation.

Previously, circumferential strain has been characterized in the AngII-induced mouse model of aortic aneurysms.[25] These analyses, however, have not been performed for mouse models of heritable thoracic aortic aneurysms, such as *FBN1*$^{mgR/mgR}$ mice. *FBN1*$^{mgR/mgR}$ mice were used in this study because of the rapid development of pronounced thoracic aneurysms.[5,26] Mouse models with mutations in *FBN1* exhibit decreased aortic elastin expression, elastin fragmentation, and TAA.[10] Aortas from WT mice experienced greater circumferential strain during systole compared

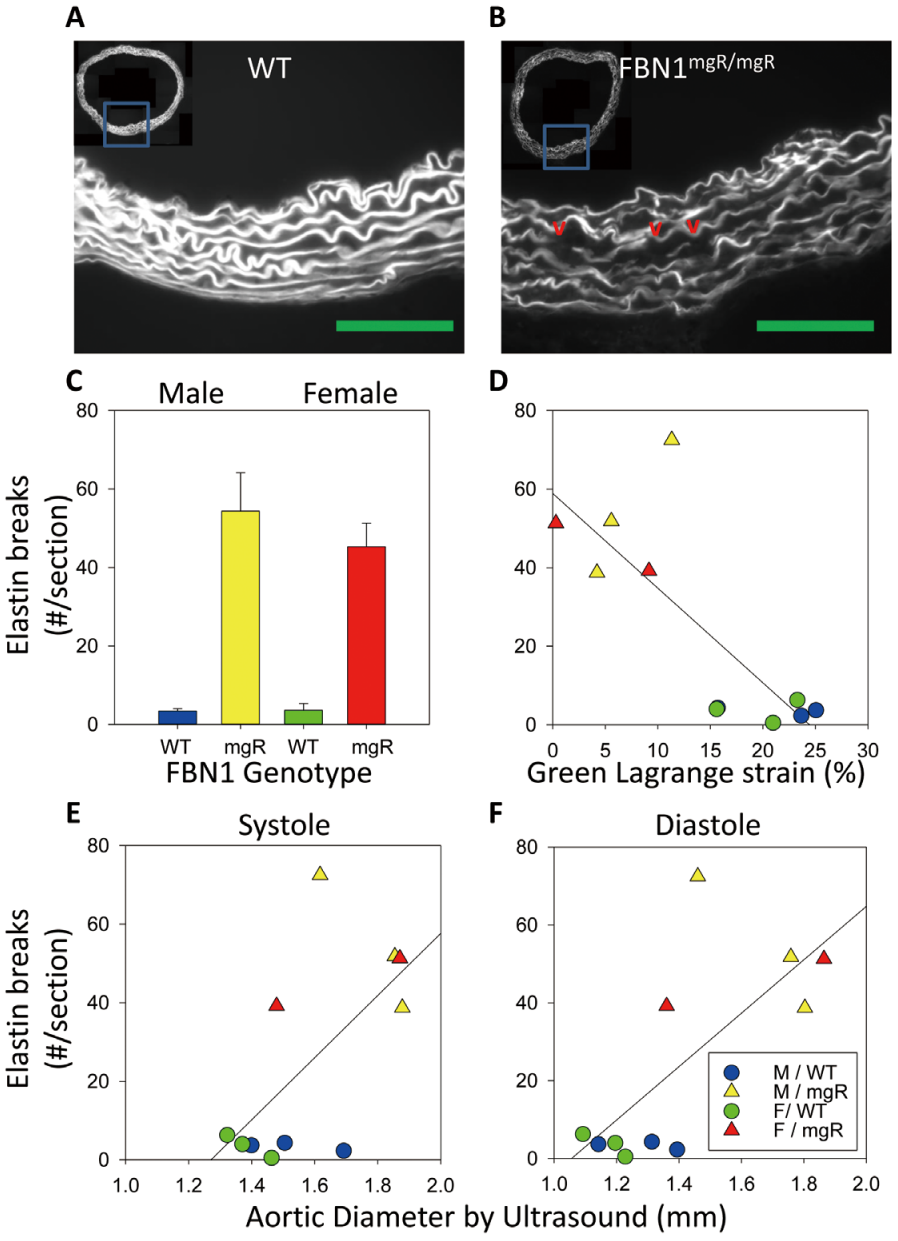

Figure 3. Elastin fragmentation of wild-type (WT) and *fibrillin-1* (*FBN1*)$^{mgR/mgR}$ correlated with ascending aortic diameter. (**A**,**B**) Representative elastin autofluorescence imaging of elastin fragmentation from WT and *FBN1*$^{mgR/mgR}$ mice at the largest ascending aortic diameter. Green line, 100μm. (**C**) Elastin fragmentation quantified. (**D**) Elastin fragmentation vs. circumferential strain (R^2=0.628, P=0.004). (**E**,**F**) Elastin breaks vs. aortic diameter in (**E**) systole (R^2=0.397, P=0.038) and (**F**) diastole (R^2=0.515, P=0.013). n=3, male WT, male mgR, female WT. n=2, female mgR.

with aortas from *FBN1*$^{mgR/mgR}$ mice. In this study, SBP was acquired using a standardized protocol on a system that measures the variance in tail volume in conjunction with a pressure cuff.[18] We have demonstrated previously that there is good correlation between blood pressure measurements obtained using this process and those obtained using telemetry.[27] Although absolute blood pressure measurements can differ between instruments, there were no differences detected in SBP between WT and *FBN1*$^{mgR/mgR}$ mice. There was also no significant difference in heart rate measured while conscious or under anesthesia. The correlation between blood pressure and circumferential strain was not significant. Blood pressures, however, were not measured during ultrasound. We cannot assume that blood pressure in the awake state is equal to blood pressure during ultrasound in the anesthetized state. Although this suggests that the increase in aortic stiffness is a function of intrinsic aortic tissue mechanics, this point merits further study. Indeed, this increase in aortic stiffness has been measured in other mouse models of spontaneous thoracic and

abdominal aortic aneurysm and dissection. Circumferential aortic strain in the AngII-induced mouse model of abdominal aortic aneurysms is approximately 15% in control mice and 5% in AngII-infused mice.[25] These strains are consistent when measured using speckle tracking technology.[28] Interestingly, AngII-induced thoracic aortic aneurysms also had reduced circumferential strain. Circumferential strains in this model decrease from 20% before infusion to 10% after AngII infusion.[29] Data from AngII-induced aortic aneurysms are in agreement with the present results in a heritable model of thoracic aortic aneurysm.

Strains have been measured ex vivo in the *FBN1*$^{mgR/mgR}$ mouse model. Previously, Lee et al demonstrated that compressive forces, measured using atomic force microscopy acting on aortas from *FBN1*$^{mgR/mgR}$ mice, produced greater deformation under stress.[10] This was attributed to the loss of elasticity in *FBN1*$^{mgR/mgR}$ aortas as evidenced by reduced area fraction of elastic fibers. We quantified elastin fragmentation as a proxy of aortic elastic behavior. While elastin fragmentation was correlated with reduced circumferential strain in response to circumferential tensile forces in vivo, this analysis is limited by the assumption that loss of continuous elastin layers leads to loss of elasticity. Paradoxically, loss of elasticity can explain both the loss of resistance to compressive forces outlined by Lee et al[10] and the increased resistance to circumferential tensile forces shown in the present study via the Poisson effect. Together, these observations imply that increased elastin fragmentation in *FBN1*$^{mgR/mgR}$ aortic tissue may be responsible for reduced aortic strain observed during systole in *FBN1*$^{mgR/mgR}$ mouse.

The primary purpose of this study was to determine the relationship between circumferential aortic strain measured in vivo and elastin fragmentation. We additionally quantified aortic diameter increases during systole compared with diastole in both WT and *FBN1*$^{mgR/mgR}$ mice. The significant size differences indicate that cardiac cycle influences interpretation of murine studies that report thoracic aortic diameters. Based on the present data, the excursion of the aorta in systole can be as great as 0.2 mm in WT aortas and 0.1 mm in aneurysmal aortas. This difference is larger than error attributable to interobserver variability in the present dataset, where bias between observers was 0.08±0.08 mm in systole and −0.07±0.06 mm in diastole (**Supplementary Figure 4**). Thus, specifying whether ascending aortic diameter was measured in either systole or diastole is especially important in order to detect small differences, ensure accuracy, and increase study power. Accounting for this phenomenon is important when ascending aortic diameter is measured across different studies. This discrepancy occurs because studies have reported aortic diameters in systole, diastole, both, or omit reporting cardiac cycle.[16,29–32] In lieu of these data, a correction factor of approximately 17% in C57BL/6J WT aortas and 5% in *FBN1*$^{mgR/mgR}$ aneurysmal aortas may be taken to approximate measurements taken in systole compared with diastole.

Conclusions

In mice that spontaneously develop elastin fragmentation, reduced circumferential strain is correlated with increased elastin fragmentation, and 2-D ultrasound data can be used to measure circumferential strain in vivo.

Acknowledgments

The authors' research work was supported by the National Heart, Lung, and Blood Institute of the National Institutes of Health under award number R01HL133723 and an American Heart Association Strategically Focus Network award number 18SFRN33900001. J.Z.C. and M.B.S. are supported by NCATS UL1TR001998. M.B.S. is also supported by the University of Kentucky College of Medicine SChoLARs Career Development Program. H.S. is supported by an AHA postdoctoral fellowship (18POST33990468). The content in this manuscript is solely the responsibility of the authors and does not necessarily represent the official views of the National Institutes of Health.

Disclosures

The authors declare no conflicts of interest.

References

1. Hiratzka LF, Bakris GL, Beckman JA, Bersin RM, Carr VF, Casey DE Jr, et al; American College of Cardiology Foundation/American Heart Association Task Force on Practice Guidelines, American Association for Thoracic Surgery, American College of Radiology, American Stroke Association, Society of Cardiovascular Anesthesiologists, Society for Cardiovascular Angiology and Interventions, Society of Interventional Radiology, Society of Thoracic Surgeons, Society for Vascular Medicine. 2010 ACCF/AHA/AATS/ACR/ASA/SCA/SCAI/SIR/STS/SVM guidelines for the diagnosis and management of patients with thoracic aortic disease: A report of the American College of Cardiology Foundation/American Heart Association Task Force on Practice Guidelines, American Association for Thoracic Surgery, American College of Radiology, American Stroke Association, Society of Cardiovascular Anesthesiologists, Society for Cardiovascular Angiography and Interventions, Society of Interventional Radiology, Society of Thoracic Surgeons, and Society for Vascular Medicine. *Circulation* 2010; **121:** e266–e369.
2. Akazawa Y, Motoki N, Tada A, Yamazaki S, Hachiya A, Matsuzaki S, et al. Decreased aortic elasticity in children with Marfan syndrome or Loeys-Dietz syndrome. *Circ J* 2016; **80:** 2369–2375.
3. Daugherty A, Rateri DL, Charo IF, Owens AP, Howatt DA, Cassis LA. Angiotensin II infusion promotes ascending aortic aneurysms: Attenuation by CCR2 deficiency in ApoE-/- mice. *Clin Sci (Lond)* 2010; **118:** 681–689.
4. Ren W, Liu Y, Wang X, Jia L, Piao C, Lan F, et al. Beta-aminopropionitrile monofumarate induces thoracic aortic dissection in C57Bl/6 Mice. *Sci Rep* 2016; **6:** 28149.
5. Pereira L, Lee SY, Gayraud B, Andrikopoulos K, Shapiro SD, Bunton T, et al. Pathogenetic sequence for aneurysm revealed in mice underexpressing fibrillin-1. *Proc Natl Acad Sci USA* 1999; **96:** 3819–3823.
6. Judge DP, Biery NJ, Keene DR, Geubtner J, Myers L, Huso DL, et al. Evidence for a critical contribution of haploinsufficiency in the complex pathogenesis of Marfan syndrome. *J Clin Invest* 2004; **114:** 172–181.
7. McLaughlin PJ, Chen Q, Horiguchi M, Starcher BC, Stanton JB, Broekelmann TJ, et al. Targeted disruption of fibulin-4 abolishes elastogenesis and causes perinatal lethality in mice. *Mol Cell Biol* 2006; **26:** 1700–1709.
8. Milewicz DM, Ostergaard JR, Ala-Kokko LM, Khan N, Grange DK, Mendoza-Londono R, et al. De novo ACTA2 mutation causes a novel syndrome of multisystemic smooth muscle dysfunction. *Am J Med Genet A* 2010; **152a:** 2437–2443.
9. Chen J, Peters A, Papke CL, Villamizar C, Ringuette LJ, Cao J, et al. Loss of smooth muscle alpha-actin leads to nf-kappab-dependent increased sensitivity to angiotensin II in smooth muscle cells and aortic enlargement. *Circ Res* 2017; **120:** 1903–1915.
10. Lee JJ, Galatioto J, Rao S, Ramirez F, Costa KD. Losartan attenuates degradation of aorta and lung tissue micromechanics in a mouse model of severe Marfan syndrome. *Ann Biomed Eng* 2016; **44:** 2994–3006.
11. Xiong W, Meisinger T, Knispel R, Worth JM, Baxter BT. Mmp-2 regulates Erk1/2 phosphorylation and aortic dilatation in Marfan syndrome. *Circ Res* 2012; **110:** e92–e101.
12. Marque V, Kieffer P, Gayraud B, Lartaud-Idjouadiene I, Ramirez F, Atkinson J. Aortic wall mechanics and composition in a transgenic mouse model of Marfan syndrome. *Arterioscler Thromb Vasc Biol* 2001; **21:** 1184–1189.

13. Howell DW, Popovic N, Metz RP, Wilson E. Regional changes in elastic fiber organization and transforming growth factor beta signaling in aortas from a mouse model of Marfan syndrome. *Cell Tissue Res* 2014; **358:** 807–819.
14. Ikonomidis JS, Gibson WC, Gardner J, Sweterlitsch S, Thompson RP, Mukherjee R, et al. A murine model of thoracic aortic aneurysms. *J Surg Res* 2003; **115:** 157–163.
15. Ikonomidis JS, Gibson WC, Butler JE, McClister DM, Sweterlitsch SE, Thompson RP, et al. Effects of deletion of the tissue inhibitor of matrix metalloproteinases-1 gene on the progression of murine thoracic aortic aneurysms. *Circulation* 2004; **110**(11 Suppl 1)**:** II268–II273.
16. Rateri DL, Davis FM, Balakrishnan A, Howatt DA, Moorleghen JJ, O'Connor WN, et al. Angiotensin II Induces region-specific medial disruption during evolution of ascending aortic aneurysms. *Am J Pathol* 2014; **184:** 2586–2595.
17. Sawada H, Chen JZ, Wright BC, Moorleghen JJ, Lu HS, Daugherty A. Ultrasound imaging of the thoracic and abdominal aorta in mice to determine aneurysm dimensions. *J Vis Exp* 2019; **145:** e59013.
18. Daugherty A, Rateri D, Hong L, Balakrishnan A. Measuring blood pressure in mice using volume pressure recording, a tail-cuff method. *J Vis Exp* 2009; **27:** e1291.
19. Goergen CJ, Barr KN, Huynh DT, Eastham-Anderson JR, Choi G, Hedehus M, et al. In vivo quantification of murine aortic cyclic strain, motion, and curvature: Implications for abdominal aortic aneurysm growth. *J Magn Reson Imaging* 2010; **32:** 847–858.
20. Preibisch S, Saalfeld S, Tomancak P. Globally optimal stitching of tiled 3D microscopic image acquisitions. *Bioinformatics* 2009; **25:** 1463–1465.
21. Barisione C, Charnigo R, Howatt DA, Moorleghen JJ, Rateri DL, Daugherty A. Rapid dilation of the abdominal aorta during infusion of angiotensin II detected by noninvasive high-frequency ultrasonography. *J Vasc Surg* 2006; **44:** 372–376.
22. Poduri A, Owens AP 3rd, Howatt DA, Moorleghen JJ, Balakrishnan A, Cassis LA, et al. Regional variation in aortic AT1b receptor mRNA abundance is associated with contractility but unrelated to atherosclerosis and aortic aneurysms. *PLoS One* 2012; **7:** e48462.
23. Rateri DL, Moorleghen JJ, Knight V, Balakrishnan A, Howatt DA, Cassis LA, et al. Depletion of endothelial or smooth muscle cell-specific angiotensin II type 1a receptors does not influence aortic aneurysms or atherosclerosis in LDL receptor deficient mice. *PLoS One* 2012; **7:** e51483.
24. Plonek T, Berezowski M, Kurcz J, Podgorski P, Sasiadek M, Rylski B, et al. The evaluation of the aortic annulus displacement during cardiac cycle using magnetic resonance imaging. *BMC Cardiovasc Disord* 2018; **18:** 154.
25. Trachet B, Fraga-Silva RA, Londono FJ, Swillens A, Stergiopulos N, Segers P. Performance comparison of ultrasound-based methods to assess aortic diameter and stiffness in normal and aneurysmal mice. *PLoS One* 2015; **10:** e0129007.
26. Pereira L, Andrikopoulos K, Tian J, Lee SY, Keene DR, Ono R, et al. Targetting of the gene encoding fibrillin-1 recapitulates the vascular aspect of Marfan syndrome. *Nat Genet* 1997; **17:** 218–222.
27. Haggerty CM, Mattingly AC, Gong MC, Su W, Daugherty A, Fornwalt BK. Telemetric blood pressure assessment in angiotensin II-Infused ApoE-/- Mice: 28 day natural history and comparison to tail-cuff measurements. *PLoS One* 2015; **10:** e0130723.
28. Favreau JT, Nguyen BT, Gao I, Yu P, Tao M, Schneiderman J, et al. Murine ultrasound imaging for circumferential strain analyses in the angiotensin II abdominal aortic aneurysm model. *J Vasc Surg* 2012; **56:** 462–469.
29. Trachet B, Piersigilli A, Fraga-Silva RA, Aslanidou L, Sordet-Dessimoz J, Astolfo A, et al. Ascending aortic aneurysm in angiotensin II-infused mice: Formation, progression, and the role of focal dissections. *Arterioscler Thromb Vasc Biol* 2016; **36:** 673–681.
30. Lee L, Cui JZ, Cua M, Esfandiarei M, Sheng X, Chui WA, et al. Aortic and cardiac structure and function using high-resolution echocardiography and optical coherence tomography in a mouse model of Marfan syndrome. *PLoS One* 2016; **11:** e0164778.
31. Shen M, Lee J, Basu R, Sakamuri SS, Wang X, Fan D, et al. Divergent roles of matrix metalloproteinase 2 in pathogenesis of thoracic aortic aneurysm. *Arterioscler Thromb Vasc Biol* 2015; **35:** 888–898.
32. Jiao Y, Li G, Li Q, Ali R, Qin L, Li W, et al. MTOR (mechanistic target of rapamycin) inhibition decreases mechanosignaling, collagen accumulation, and stiffening of the thoracic aorta in elastin-deficient mice. *Arterioscler Thromb Vasc Biol* 2017; **37:** 1657–1666.

Supplementary Files

Please find supplementary file(s);
http://dx.doi.org/10.1253/circrep.CR-18-0012